JACS
JOURNAL OF THE AMERICAN CHEMICAL SOCIETY
pubs.acs.org/JACS
Article

Chemisorption-Induced Formation of Biphenylene Dimer on Ag(111)

Zhiwen Zeng,[⬡] Dezhou Guo,[⬡] Tao Wang,* Qifan Chen, Adam Matěj, Jianmin Huang, Dong Han, Qian Xu, Aidi Zhao, Pavel Jelínek, Dimas G. de Oteyza, Jean-Sabin McEwen,* and Junfa Zhu*

Cite This: J. Am. Chem. Soc. 2022, 144, 723−732
Read Online
ACCESS | Metrics & More | Article Recommendations | Supporting Information

ABSTRACT: We report an example that demonstrates the clear interdependence between surface-supported reactions and molecular-adsorption configurations. Two biphenyl-based molecules with two and four bromine substituents, i.e., 2,2′-dibromobiphenyl (DBBP) and 2,2′,6,6′-tetrabromo-1,1′-biphenyl (TBBP), show completely different reaction pathways on a Ag(111) surface, leading to the selective formation of dibenzo[*e*,*l*]pyrene and biphenylene dimer, respectively. By combining low-temperature scanning tunneling microscopy, synchrotron radiation photoemission spectroscopy, and density functional theory calculations, we unravel the underlying reaction mechanism. After debromination, a biradical biphenyl can be stabilized by surface Ag adatoms, while a four-radical biphenyl undergoes spontaneous intramolecular annulation due to its extreme instability on Ag(111). Such different chemisorption-induced precursor states between DBBP and TBBP consequently lead to different reaction pathways after further annealing. In addition, using bond-resolving scanning tunneling microscopy and scanning tunneling spectroscopy, we determine with atomic precision the bond-length alternation of the biphenylene dimer product, which contains 4-, 6-, and 8-membered rings. The 4-membered ring units turn out to be radialene structures.

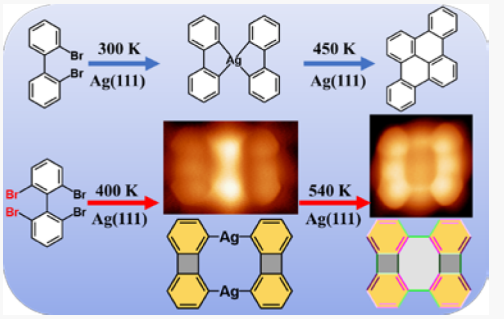

INTRODUCTION

On-surface synthesis (OSS) has shown its great potential in the fabrication of functional molecules and covalent nanostructures with atomic precision in the past decade.[1−3] Different from solution-phase chemistry because of the required clean reaction environment (ultrahigh vacuum) at the gas−solid interface, the use of catalysts are largely limited in OSS. Hence, steering reaction pathways in OSS has been more challenging overall than in wet chemistry. Chemical organic reactions on surfaces typically include three basic steps: molecular adsorption, diffusion, and reaction. The reported examples toward steering reaction pathways on surfaces were mostly focused on tuning the molecular diffusion and the reaction barriers.[1−3] For instance, it has been demonstrated that self-assembly templates can efficiently direct the reaction pathways by confining molecular diffusion.[4−7] In addition, different metal substrates or metal adatoms normally have a different catalytic activity toward a specific on-surface reaction, thus impacting the reaction barriers.[8−11] However, related studies on the adsorption process are rare, although it actually differentiates the heterogeneous on-surface synthesis from the homogeneous solution-phase chemistry. A few reported examples were focused on the physisorption of intact molecules on surfaces. The adsorption height from the surface[12] and the adsorption site[13] can play important roles on the reactivity of the functional groups of precursor molecules.

The coupling reactions typically involve the generation and coupling of radicals and have been extensively studied.[2,14,15] Radicals are generated when functional groups are activated. The adsorption configuration of newly formed radical species is very different from that of the initial molecule because active radical species are normally stabilized by surface atoms or stray surface adatoms.[16] Thus, the adsorption configurations of the activated molecules are largely determined by their radical sites. As a result, it is reasonable to infer that molecules with the same backbone but a different number of radicals may lead to a dramatically different adsorption behavior on surfaces after activation. In turn, the different adsorption behaviors may potentially influence the reaction pathways and the final products.

Herein, we report such an example by comparing the reactions of 2,2′-dibromobiphenyl (DBBP) and 2,2′,6,6′-tetrabromo-1,1′-biphenyl (TBBP) molecules on a Ag(111)

Received: August 7, 2021
Published: December 29, 2021

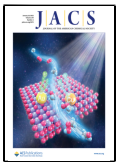

Downloaded via WASHINGTON STATE UNIV on June 5, 2022 at 19:15:26 (UTC).
See https://pubs.acs.org/sharingguidelines for options on how to legitimately share published articles.

ACS Publications
© 2021 American Chemical Society

https://doi.org/10.1021/jacs.1c08284
J. Am. Chem. Soc. 2022, 144, 723−732

surface (Scheme 1). In our previous work,[17] we showed that the biradical biphenyl species formed upon debromination of DBBP were efficiently stabilized by surface Ag adatoms at 300 K. Further annealing led to the formation of dibenzo[*e*,*l*]-pyrene nanographene. However, in this work, TBBP shows a unique reaction pathway: The first step involves the generation of four-radical biphenyl species after the debromination of the precursor. Then TBBP undergoes intramolecular annulation spontaneously at 300 K due to its extreme instability on Ag(111), forming a biradical biphenylene monomer that is anchored to the surface. Further annealing leads to the formation of an organometallic intermediate state, followed by its transformation into covalent biphenylene dimers containing 4-, 6-, and 8-membered carbon rings. The chemical structure and electronic properties of the biphenylene dimer have been studied by bond-resolving scanning tunneling microscopy (BR-STM) and scanning tunneling spectroscopy (STS), offering significant insights into its potential antiaromaticity. The

Scheme 1. Reaction Pathways of (a) DBBP and (b) TBBP on the Ag(111) Surfaces

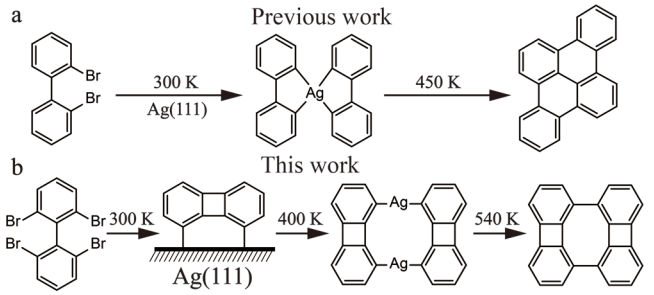

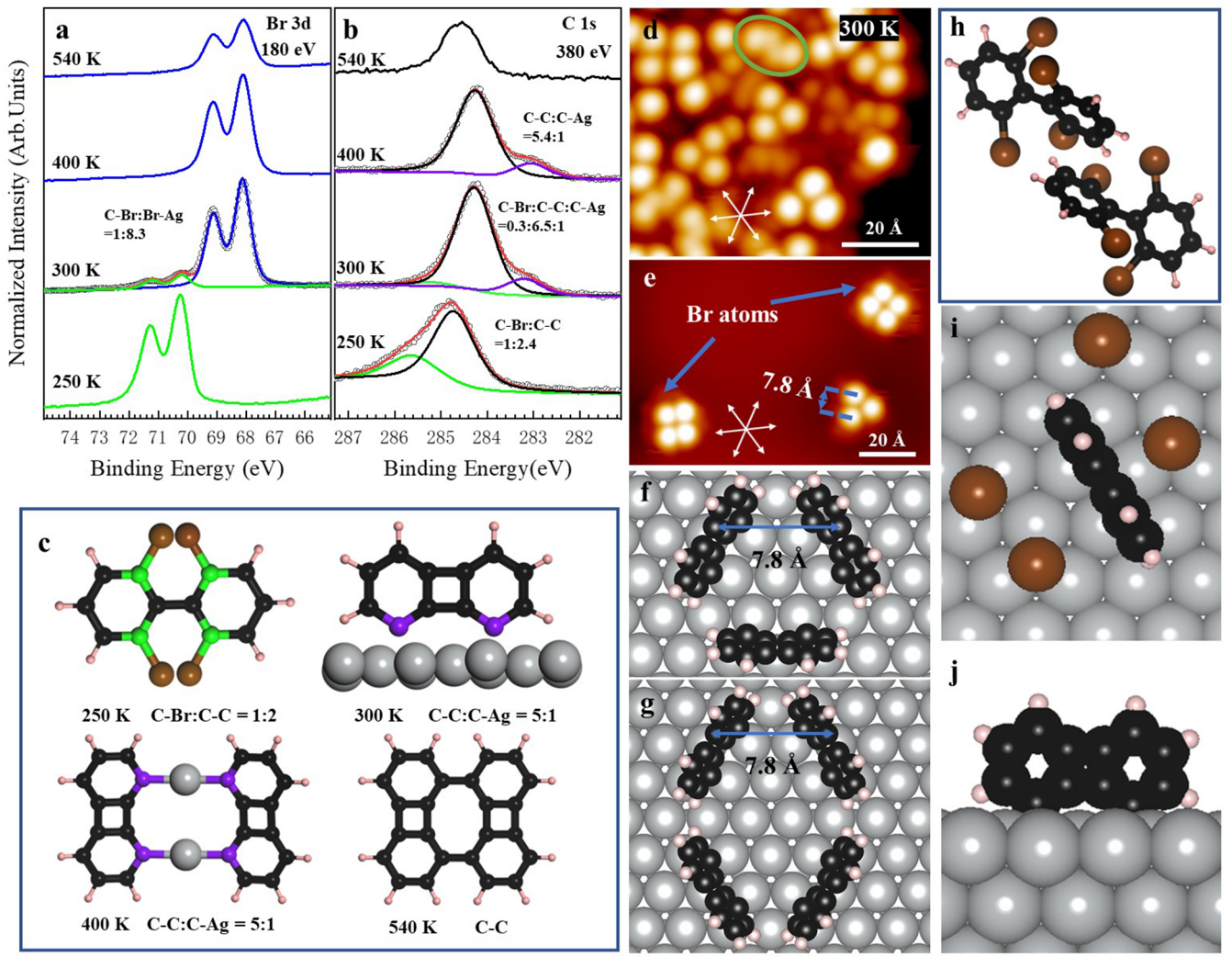

Figure 1. (a) Br 3d and (b) C 1s SRPE spectra of the samples prepared by depositing TBBP on Ag(111) held at 250 and 300 K followed by annealing to 400 and 540 K. The photon energies for Br 3d and C 1s are 180 and 380 eV, respectively. (c) Molecular models of the major products at each temperature. Different carbon atoms (black, green, and purple spheres) are depicted by different colors to illustrate their chemical environments. The ideal ratios of these C atoms are shown below each molecular model. (d, e) STM images of the sample upon deposition of TBBP on Ag(111) held at 300 K. The three high symmetric directions of the Ag(111) surface are shown as the white arrows; the same holds for the following overview STM images. Tunneling parameters: $U = -1.5$ V, $I = 50$ pA. DFT-calculated structural model of (f) the trimer and (g) the tetramer as depicted in part (e). (h) Possible structural model of two TBBP molecules in the green circle of (d). (i, j) Top and side views of DFT optimized structure of debrominated TBBP adsorbing on Ag(111). Color code: C, black; Ag, gray; H, pink; Br, brown; C bonded to Br atom, green; C bonded to Ag atom, purple.

https://doi.org/10.1021/jacs.1c08284
J. Am. Chem. Soc. 2022, 144, 723−732

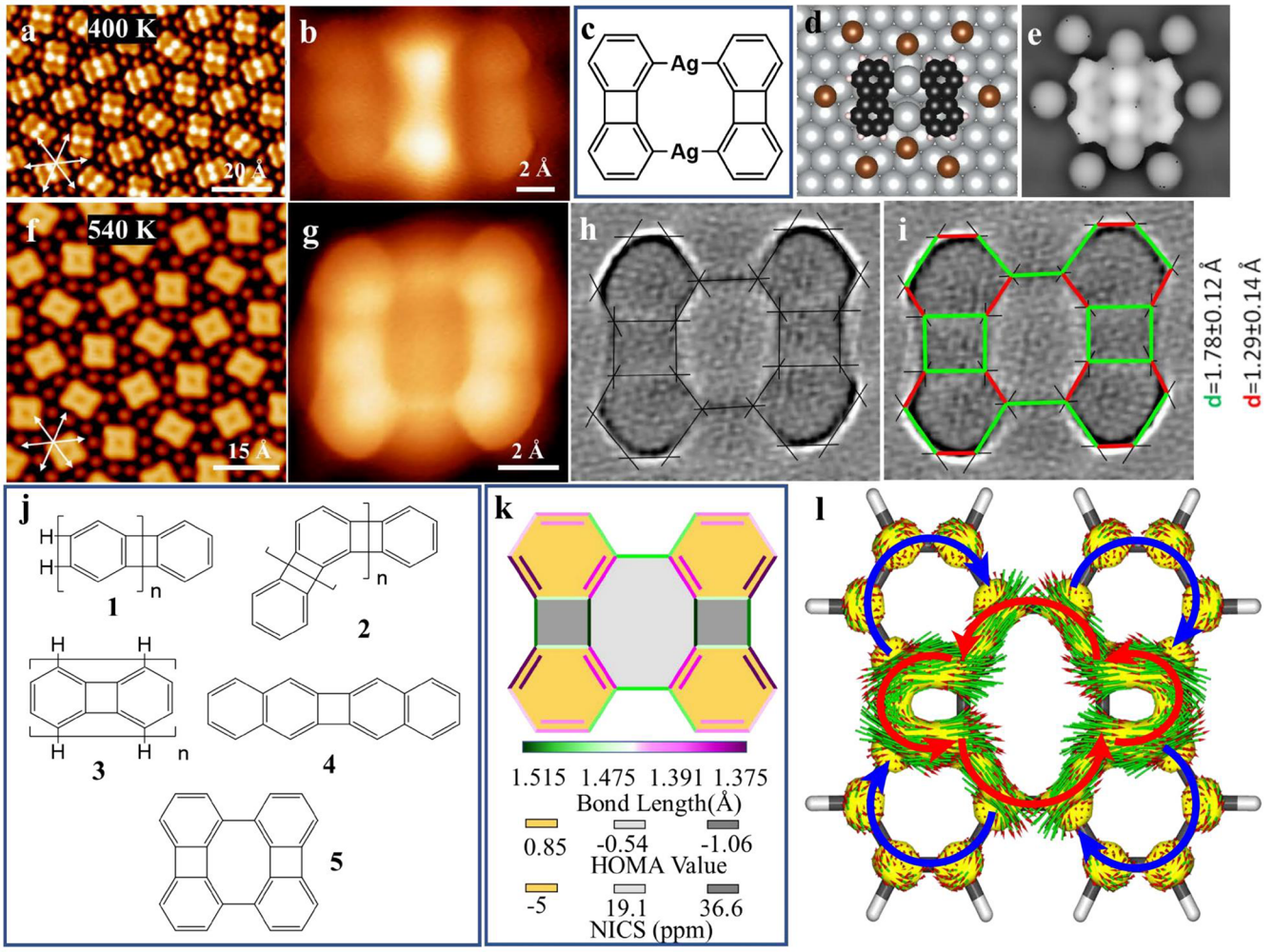

Figure 2. (a, b) Overview and constant-height BR-STM images of the organometallic dimer covered sample after annealing the 300 K sample to 400 K. (c−e) Structural model, DFT-optimized structure, and simulated STM image of the organometallic dimer, respectively. (e) U_{bias} is set to −0.1 V. (f) Overview and (g) constant-height BR-STM images of the sample after further annealing to 540 K. Tunneling parameters: (a) U = −0.1 V, I = 1.5 nA; (b) U = 5 mV; (f) U = 0.1 V, I = 1.2 nA; (g) U = 5 mV. (h, i) Corresponding Laplace filtered image of (g) for a better view of the bonds. The average length for the single bonds (marked in green in panel (i)) is 1.78 ± 0.12 Å, whereas the average length for the double bonds (marked in red in panel (i)) is 1.29 ± 0.12 Å. (j) Chemical structures of some biphenylene derivatives showing the bond alternations. (k) DFT calculated C−C bonds lengths and HOMA (on surface) and NICS (in gas phase) values of the biphenylene dimer, represented by gradient colors as indicated. The phenyl rings in the biphenylene dimer have a HOMA value of 0.85 and an NICS value of −5 ppm, while the 8-membered and 4-membered rings have HOMA values of −0.54 and −1.06 and NICS values of 19.1 and 36.6 ppm, respectively. (l) ACID analysis of biphenylene dimer calculated in the gas phase (red and blue darts show orientation of the peripheral ring current along 4-, 8- membered rings and phenyl rings, respectively).

mechanism for the different reaction selectivities between DBBP and TBBP, i.e., the formation of dibenzo[*e*,*l*]pyrene versus a biphenylene dimer, has been further elucidated through a density functional theory (DFT)-based model. This work reveals that the chemisorption behavior of adsorbates can play a decisive role on the reaction pathway. In addition, the bond alternation of the intriguing biphenylene dimer,[18] as proposed by organic and theoretical chemists, has been corroborated here in real space. In fact, the fabrication of 4-membered ring-containing structures on surfaces has become an important topic and has been widely studied recently due to their exotic electronic and mechanical properties, which can be achieved by either intramolecular or intermolecular annulation reactions.[19−26] An outstanding example was reported by Fan et al.[24] In that work, the biphenylene network with periodically arranged 4-, 6-, and 8-membered rings was synthesized by an interpolymer hydrogen−fluoride zipping reaction and exhibited metallic electronic properties. The chemisorption-induced formation of the 4-membered ring as presented in our work provides new insights into the fabrication of 4-membered ring-containing functional nanostructures on surfaces.

RESULTS AND DISCUSSION

Synthesis of Biphenylene Dimer. Figure 1 presents our experimental results of TBBP molecules adsorbing on Ag(111) at room temperature. TBBP molecules stayed intact on Ag(111) at ∼250 K, as revealed by the Br 3d and C 1s synchrotron radiation photoemission (SRPE) spectra in parts a and b of Figure 1, respectively. The ratio between C−Br and C−C was 1:2.4, in fair agreement with the ideal value of 1:2 as derived from the structural model shown in Figure 1c. The corresponding STM images are shown in Figure S1. The molecules self-assembled into square ordered islands. A single molecule was composed of one bright head (yellow dotted

https://doi.org/10.1021/jacs.1c08284
J. Am. Chem. Soc. 2022, 144, 723−732

contour) and one weak tail (green dotted contour), indicating that its twisted adsorption configuration was due to the repulsion between the adjacent Br atoms of intact TBBP.[15,27]

After depositing TBBP molecules onto the Ag(111) surface held at 300 K, packs of bright protrusions were exhibited in the STM images, as shown in Figure 1d and e (an overview STM image is shown in Figure S2). Most molecules aggregated into close-packed islands (Figure 1d), together with a few sparsely distributed trimers and tetramers (Figure 1e). In particular, the existence of the trimer (Figure 1e) implies that the bright protrusion could not be from a submolecular feature, i.e., one protrusion could not correspond to one phenyl group of TBBP. In addition, the center-to-center distance between adjacent bright protrusions was measured to be 7.8 Å, which was much larger than the distance between the two phenyls of TBBP (~4.3 Å). Therefore, one bright protrusion could only correspond to one individual TBBP molecule. The majority of C−Br bonds of TBBP were dissociated at 300 K, as evidenced by the downward shift of the Br 3d core-level binding energies from 250 to 300 K.[28] The partial dissociation of C−Br bonds on Ag(111) was also reported by previous works.[2,29,30] The Br adatoms on the surface can be recognized as the relatively dark and small dots in the STM images,[6,31] as pointed out by the blue arrows in Figure 1e. Interestingly, the appearance of a new C 1s component at a low binding energy of 283.0 eV at 300 K (Figure 1b) implies that radicals were probably stabilized by the surface atoms via a C−Ag coordination.[28,31] The ratio between C−Ag and C−C was ~1:6 from the C 1s spectrum (C−Br/C−C/C−Ag = 0.3:6.5:1), implying that only 2 out of 12 carbon atoms of TBBP which hold radicals were coordinated to the surface atoms (ideally C−Ag: C−C=1:5). It is worth noting that the the C 1s core level binding energy shifts toward lower energy values at 300 K with respect to that at 250 K was attributed to the increase of the surface work function induced by chemisorbed Br adatoms on the surface.[28,29,32−34] Inspired by these findings and related previous works,[35] one can intuitively deduce that the four-radical biphenyl underwent intramolecular annulation reactions at 300 K, forming biphenylene, while the two residual unquenched radicals were stabilized by the Ag surface (Figure 1c). Consequently, it adsorbed perpendicularly to the surface, as schematically shown in Scheme 1 and Figure 1c. This is why the adsorbates showed such bright features as compared to that of conventional flat molecules that adsorb parallel to the surface. A comparison between the apparent height of the biradical biphenylene monomer and the final biphenylene dimer product on Ag(111) is presented in Figure S3, where a difference of 1.8 Å was obtained. The perpendicular adsorption configuration also explained the formation of trimers and tetramers in parts d and e of Figure 1, respectively, which should be stabilized by $\pi-\pi$ stacking between face-to-face phenyls.[36−38] The DFT-calculated structural models of the trimer and the tetramer are displayed in parts f and g of Figure 1, respectively. The distance between two adjacent molecules was ~7.8 Å for both the trimer and the tetramer, which was in excellent agreement with the experimental value (Figure 1e). The formation of the biphenylene dimer was verified by our DFT calculations. Once the TBBP molecules were fully debrominated, four-radical biphenyl species were not stable on the Ag surface but immediately started an intramolecular annulation reaction (Figure 1i and j). As a result, a biphenylene complex was formed with two radicals binding with two surface silver atoms, leading to the nonradical side of the benzene ring pointing away from the surface. We tested various adsorption sites of the Ag(111) surface with biphenylene (as shown in Figures S9 and S10) and found that two radicals preferred to bind with two nearby surface Ag atoms rather than with the Ag adatom.

Note that a few C−Br bonds remained intact at 300 K from the X-ray photoelectron spectroscopy (XPS) analysis, which could belong to the molecules inside the green circle in Figure 1d because of their similar STM morphology as the intact molecules at 250 K (Figure S1). Although the possibility that one or more Br atoms were lost on these molecules could not be excluded, these molecules could most likely be attributed to intact TBBP. Because the $\pi-\pi$ stacking interactions between TBBP and the neighboring biradical biphenylenes (Figure 1d) were different from the $\pi-\pi$ interactions in the ordered TBBP island at 250 K (Figure S1), the morphology of TBBP in the STM images could be slightly different.[39,40] Figure 1h shows the corresponding structural model of the two molecules in the green circle in Figure 1d.

Upon annealing the sample at 400 K, large-area close-packed islands composed of organometallic dimers were obtained, as shown in Figure 2a (an overview STM image is shown in Figure S4). This was presumably attributed to the planarization of biradical biphenylenes on the surface, where two C−Ag−C linkages were formed as expected (Figure 2c).[41] The BR-STM image using a CO-functionalized probe[42] corroborated the structure, as shown in Figure 2b. The two bright dots in the middle were assigned to two Ag adatoms, while the darker sides were biphenylenes. In addition, the DFT-calculated structural model (Figure 2d) and simulated STM image (Figure 2e) both fit the experimental result well. The formation of an organometallic dimer was also supported by the C 1s SRPE spectrum, which is deconvoluted into C−C and C−Ag components with a ratio of 5.4:1, in good agreement with the proposed molecular structure (ideally 5:1, as derived from the structural model shown in Figure 1c). At these conditions, TBBP completes its fully debromination process (see Br 3d SRPE spectra in Figure 1a). Br adatoms imaged as relatively dark dots surrounding the organometallic dimer via Br···H hydrogen bonds (Figure 2a).[41]

Further annealing this sample at 540 K triggered the formation of the final covalent product biphenylene dimer (Figures 2f and S4) after the removal of interstitial Ag adatoms from the organometallic dimers. The submolecular structure was clearly characterized by the BR-STM with a CO-functionalized probe, as seen in Figure 2g. The covalent connection between two monomers was further confirmed by C 1s SRPE spectra, where the C−Ag signal disappeared at 540 K (Figure 1b). Because the annealing from 400 to 540 K led to the partial desorption of Br atoms as revealed in the Br 3d spectra, the C 1s peak shifted back to the high-binding-energy position at 540 K.[28,29,32−34]

Chemical Structure of Biphenylene Dimer. The biphenylene dimer is of particular interest for studying molecular antiaromaticity because it is a 4-, 6-, and 8-membered ring-containing structure.[18,24,43] A cyclic molecule typically shows antiaromaticity if it holds $4n$ (n is a positive integer) delocalized electrons, while a cyclic molecule containing $4n + 2$ delocalized electrons is aromatic.[44] In particular, cyclobutadiene is thought to be very antiaromatic and not stable. Plenty of theoretical and experimental efforts (mostly crystallography) have been made to study the bond alternation of several biphenylene derivatives.[18,45−51] A few

https://doi.org/10.1021/jacs.1c08284
J. Am. Chem. Soc. 2022, 144, 723−732

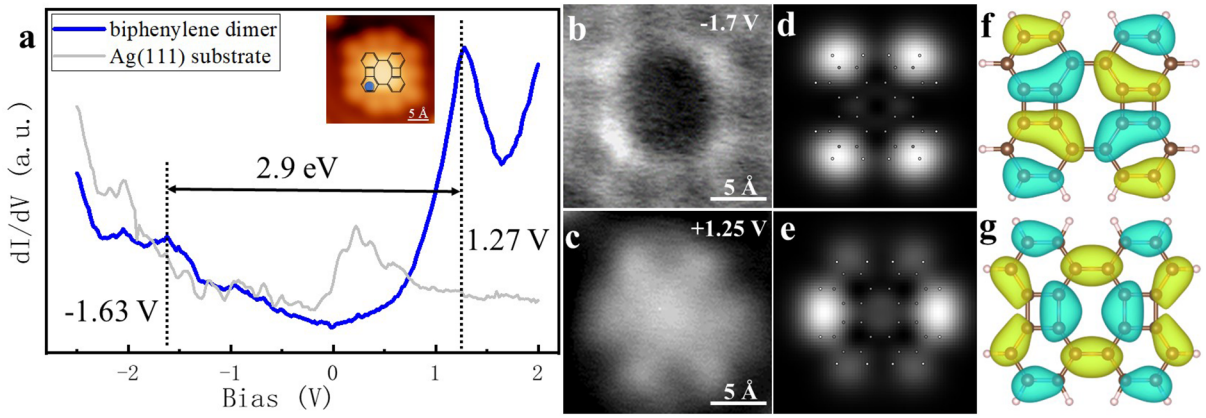

Figure 3. Electronic properties of biphenylene dimer on Ag(111). (a) Differential conductance (dI/dV) spectra. The blue curve shows the dI/dV spectrum recorded at the position on the molecule marked with a blue dot, with a Br-functionalized tip. The gray curve shows the reference dI/dV spectrum measured on the bare Ag(111) surface with the same tip. The 10 dots surrounding the molecule are 10 bromine adatoms. Lock-in amplitude, 20 mV; oscillation frequency, 731 Hz. (b, c) Constant-current dI/dV maps taken at the bias voltages of −1.7 and 1.25 V, respectively. Lock-in amplitude, 20 mV; oscillation frequency, 731 Hz; current, 500 pA. (d, e) DFT-based dI/dV maps corresponding to HOMO and LUMO of a biphenylene dimer in the gas phase at an isosurface level of 0.05 $Bohr^{-3/2}$, respectively. (f, g) DFT-based LDOS distribution of HOMO and LUMO orbitals of biphenylene dimer in the gas phase, respectively. Electron orbitals are presented by blue isosurfaces for negative phase values and by yellow isosurfaces for positive phase values.

typical examples are shown in Figure 2j. The linear polyphenylene **1** showed delocalized electronic properties, and one double bond could be involved inside the 4-membered ring. In contrast, the angular polyphenylene **2** and oligobiphenylenes **3** possessed localized π-bonding and held radialene structures. The double bonds tended to be exocyclic with respect to the 4-membered rings in **2** and **3** to minimize the antiaromatic character of 4-electron π-bonding within the cyclobutadiene.

The first real-space evidence for the bond alternation of the biphenylene-related structure was given by Kawai et al. by analyzing the bond lengths of molecule **4** using noncontact atomic force microscopy (nc-AFM).[35] Here we demonstrate that the bond alternation of biphenylene dimer **5** was similar to that of biphenylene monomer, that is, the radialene structure was energetically favorable. A Laplace-filtered BR-STM image, which enhances the bond feature, is presented in Figure 2h.[52] We drew the best-fitting straight lines along the different bonds of the molecular structure and took the crossing points as reference for the bond-length analysis. Remarkably large differences in the bond lengths could be easily identified, that is, those predicted to display a double-bond character were clearly shorter. A detailed analysis (Figure 2i) revealed that the average length for the single bonds (marked in green) was 1.78 ± 0.12 Å, whereas the average length for the double bonds (marked in red) was 1.29 ± 0.12 Å, clearly out of the error range of one another. We note that these values were not the actual bond lengths. However, the artifact that caused these lengths to deviate from the real values was strongly bond-order dependent, which thus allowed for an easy discrimination of the single and double bonds by this comparative analysis.[53] We also calculated the length of each C−C bond of the biphenylene dimer adsorbed on the Ag(111) surface and derived the harmonic oscillator model of aromaticity (HOMA) values (Figure 2k).[54] A higher HOMA value was generally associated with a higher degree of π-electron delocalization and increased aromatic stabilization. The phenyl rings had the highest HOMA value of 0.85. The 8- and 4-membered rings had HOMA values of only −0.54 and −1.06, respectively, indicating their low aromaticities. This was presumably because of the single bonds involved there, which decreased the π-electron delocalization on them. Nevertheless, the HOMA value of the 4-membered ring was still much higher than the value of cyclobutadiene (−4.277), which indicated that the antiaromaticity in the 4-membered ring was significantly reduced in the biphenylene dimer.[54] This was further supported by the nuclear-independent chemical shift (NICS) analysis,[55] as shown in Figure 2k. The phenyl rings were rather quasi-nonaromatic (−5 ppm), while the 4- and 8-membered rings were highly antiaromatic (36.6 and 19.1 ppm, respectively). In addition, we investigated the induced currents that resulted from an applied magnetic field by the anisotropy of the induced current density (ACID).[56] The plot depicted in Figure 2l clearly shows a high anticlockwise current flowing along the central rings including both 4- and 8-membered rings, which suggested the antiaromaticity of the 4- and 8-membered rings. In contrast, only a fragmented clockwise ring current (weak aromaticity) was shown in the phenyl rings, in agreement with their low NICS values. The reduced aromaticity of the phenyl ring was due to the fixed localization of the double bonds caused by the 4-membered rings.

Electronic Structure of Biphenylene Dimer. The electronic properties of the biphenylene dimer adsorbed on Ag(111) were probed by STS, as shown in Figure 3a. The two peaks at −1.63 and 1.27 V were attributed to the highest occupied and lowest unoccupied molecular orbitals (HOMO and LUMO), respectively. This was supported by the good agreement between the experimentally obtained (Figure 3b and c) and DFT-simulated dI/dV maps of the HOMO and LUMO (Figure 3d and e) of the biphenylene dimer (the 10 dark rings in Figure 3b are from the contribution of the surrounding Br adatoms). Because the STS signal at the negative bias was not as strong as the positive one, we further obtained constant-height dI/dV maps at different negative bias voltages, as shown in Figure S5. The dI/dV map obtained at −1.7 V nicely matched the simulation. Instead, the HOMO signal became less prominent as the bias voltage was ramped toward the in-gap values. This was shown, e.g., with bias values

https://doi.org/10.1021/jacs.1c08284
J. Am. Chem. Soc. 2022, 144, 723−732

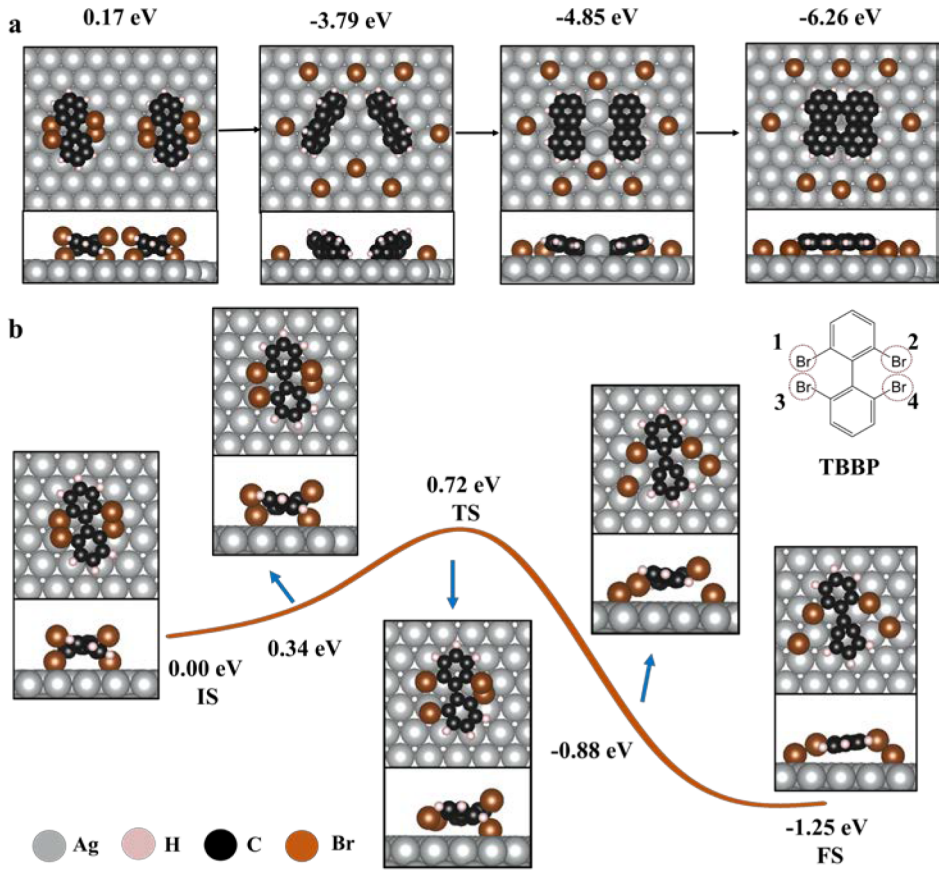

Figure 4. (a) Optimized configurations of the reaction evolution of TBBP to biphenylene dimer on Ag(111). The energy values shown in each structure are calculated with eq S3 as shown in the Supporting Information, where the total energy of a TBBP monomer adsorbate is taken as a reference for the comparison between the different adsorbates. (b) Energy diagram of the initial debromination reaction of TBBP on Ag(111). The initial state, transition state, and final state are denoted as IS, TS, and FS, respectively. The structure model of TBBP is shown in the upper right corner, in which four bromine atoms are marked by dashed red circles. The total energy of the initial state is taken as a reference (set as 0). Color code: C, black; Ag, gray; H, pink; Br, brown.

of −1.4 and −1.2 V, which showed a decreasing contribution from the HOMO and rather mirrored the molecular structure and the associated modifications of the tip−sample transmission function as the probe was scanned at constant height above the molecule. This evolution of the conductance signal confirmed that the dI/dV signal at −1.7 V corresponded to the HOMO of the biphenylene dimer. On the basis of this, the band gap of the biphenylene dimer adsorbed on Ag(111) was 2.9 eV, which was larger than that of the biphenylene ribbon (2.35 eV on Au(111)), as reported by Fan et al.,[24] due to its smaller size. The relatively large bandgap was presumably attributed to the relatively large electronic localization on the phenyl groups (weak electronic conjugation between them). The calculated electronic local density of states (LDOS) distributions related to the HOMO and LUMO orbitals of the biphenylene dimer are presented in Figure 3f and g. Accordingly, the HOMO was largely localized in the phenyl groups, while the LUMO was mostly distributed in the 4-membered ring and the single bond between two biphenylene monomers, thus fitting the proposed bond alternation well, as shown in Figure 2k. The DFT-calculated charge densities of the HOMO and LUMO of the biphenylene dimer adsorbing on Ag(111) are presented in Figure S11, and they are very similar to those in the gas phase as shown in Figure 3f and g, implying a weak interaction between the biphenylene dimer and the Ag(111) surface.

Reaction Pathway Analysis. Next, we focused on the reaction mechanisms of TBBP and DBBP on Ag(111). The optimized structures from a DFT-based model for each reaction step of TBBP are shown in Figure 4a. The details of these calculations are given in the Supporting Information.

As shown in Figure 4a, the reaction of TBBP was an exothermic reaction where the energy diagram went downhill in each reaction step. Notably, the first step was an adsorption-determined spontaneous process, which was also reflected by the considerable heat release of 3.96 eV. After full debromination of TBBP, the intramolecular annulation reaction of the four-radical biphenyl turned out to be the most thermodynamically favorable pathway. This was supported by the fact that the energy of Ag−biphenyl complex, as another possible structure, was 3.75 eV higher than that of the biphenylene monomer product on Ag(111), as seen in Figure S16. In fact, the energy barrier of the intramolecular annulation of TBBP on Ag(111) should be from the debromination reaction of TBBP. As shown in Figure 4b, two Br atoms on the same benzene ring (either sites 1 and 2 or sites 3 and 4) preferred dissociating simultaneously with an energy barrier of 0.72 eV and an exothermic reaction energy of 1.25 eV. This excluded the possibility that the intramolecular annulation might also occur as long as two bromines dissociated on the same side (either sites 1 and 3 or sites 2 and 4) of the molecular backbone (instead of full

https://doi.org/10.1021/jacs.1c08284
J. Am. Chem. Soc. 2022, 144, 723−732

debromination). Detailed descriptions of these calculations are shown in Figure S15. The following steps were the conventional planarization of the biradical biphenylene monomer with the help of Ag adatoms and the subsequent Ullmann coupling by thermal treatments, finally forming the biphenylene dimer.

In contrast, for the reaction of DBBP on Ag(111), the reaction was an Ullmann coupling followed by the cyclodehydrogenation, forming dibenzo[*e*,*l*]pyrene (Scheme 1). It was obvious that the difference between the two reactions (TBBP and DBBP) on Ag(111) originated from different molecular adsorption configurations. Different from the spontaneous annulation of TBBP, in the case of DBBP, both the Ag surface and the Ag adatoms were adequate to stabilize the biradical biphenyl, resulting in the formation of an organometallic dimer with 4-fold C−Ag bonds (Figure S19). It is known that Ullmann coupling has a very low reaction barrier after the removal of interstitial Ag atoms from an organometallic intermediate;[57−59] thus, the formation of dibenzo[*e*,*l*]pyrene was expected. Each reaction step of DBBP on Ag(111) was an exothermic reaction, as seen in Figure S19.

It is worth noting that the intramolecular annulation reaction of biradical biphenyl should be possible after the removal of Ag atoms from the organometallic dimer. However, a much higher temperature was needed for the intramolecular annulation of the biradical biphenyl. For example, in the work of Kawai et al., intramolecular annulation to form **4**, as shown in Figure 2j, could be achieved only at temperatures higher than 406 K.[35] The energy barrier of intramolecular annulation of the biradical biphenyl thus should be higher than that of the Ullmann coupling between radicals (usually <1 eV; demetallization was normally the rate-determining step of the Ullmann reaction on surfaces),[58,59] which related to the planarization of the molecule on the Ag(111) surface. The relatively high barrier of intramolecular annulation of DBBP on Ag(111) was also supported by the experimental results. First of all, annealing of DBBP on Ag(111) at 450 K led to the formation of only dibenzo[*e*,*l*]pyrene, and no biphenylene products were observed. However, one could argue that the self-assembly template effect of an organometallic dimer island might enhance the Ullmann coupling, which took place through a molecular transition and prohibited the intramolecular annulation that occurred by molecular rotation.[5,60] Therefore, we performed control experiments by depositing DBBP molecules on the hot Ag(111) surfaces to avoid the self-assembly template effects. The results showed that the products were still almost 100% dibenzo[*e*,*l*]pyrene by 450 K hot deposition (Figure S6). The biphenylene monomer from the intramolecular annulation could appear as a very minor byproduct only when the deposition was employed on a hotter sample (550 K), together with some other byproducts (Figure S7). This was because the deposition on a very hot sample could normally overcome some high reaction barriers.[6,61,62] Nevertheless, the total yield of these byproducts was <10% and dibenzo[*e*,*l*]pyrene still dominated, thus supporting the point that the energy barrier of the Ullmann coupling of DBBP on Ag(111) was much lower as compared to that of intramolecular annulation.

In short, the main reason for the different reaction pathways of TBBP and DBBP on Ag(111) was their different chemisorption configurations. The four-radical biphenyl required a spontaneous intramolecular annulation to lower the overall energy. In sharp contrast, the biradical biphenyl could be easily stabilized by the surface adatoms. In addition, intramolecular annulation of DBBP was less favored than the competing Ullmann coupling, thus leading to its completely different reaction selectivity on Ag(111) as compared to TBBP. To investigate the generality of the chemisorption-induced reaction selectivity of TBBP on metal surfaces, we further studied the reaction of TBBP on the Ag(100) surface. Biphenylene dimers were also selectively obtained on Ag(100) by undergoing an organometallic intermediate state, identical to the reaction pathway of TBBP on Ag(111), as shown in Figure S8.

CONCLUSIONS

In summary, biphenylene dimers are selectively synthesized on a Ag(111) surface with a high yield, starting from TBBP. Using BR-STM and STS, we demonstrate that the radialene rather than a cyclobutadiene structure is preferred in the biphenylene dimer. The high selectivity toward a biphenylene dimer is attributed to the special adsorption configuration of TBBP on Ag(111). After debromination, the four-radical biphenyl cannot be stabilized simply with the help of surface atoms and instead undergoes an intramolecular annulation reaction and finally forms a biphenylene dimer via intermolecular Ullmann coupling. In contrast, the biradical biphenyl from the debrominations of DBBP can be efficiently stabilized by surface Ag adatoms, forming an organometallic dimer. This organometallic intermediate subsequently reacts into dibenzo[*e*,*l*]pyrene via Ullmann coupling. Control experiments demonstrate that the energy barrier of intramolecular annulation reaction is higher than that of the Ullmann coupling reaction for the biradical biphenyl on Ag(111). The different adsorption configurations on Ag(111) lead to different reaction pathways for the two structurally similar adsorbates. We believe this work can invoke scientists' interests because it serves as an example of how one can control the reaction selectivity for a given adsorbate by tuning its adsorption behavior.

More interestingly, on the basis of STS and the combined HOMA, NICS, and ACIDS analyses, we provide comprehensive interpretations toward the antiaromaticities of 4- and 8-membered rings that contain 4*n* electrons. In addition, because of the bond-confinement caused by the existence of the 4-membered ring, the aromaticity of phenyl is significantly reduced. The bond-confinement effect revealed here could be potentially employed for other graphene-based and non-benzenoid carbon structures, tuning the electronic properties and chemical reactivity of these materials.

ASSOCIATED CONTENT

Supporting Information

The Supporting Information is available free of charge at https://pubs.acs.org/doi/10.1021/jacs.1c08284.

Detailed descriptions of experimental and theoretical methods and additional STM images (PDF)

AUTHOR INFORMATION

Corresponding Authors

Tao Wang − *National Synchrotron Radiation Laboratory, Department of Chemical Physics and Key Laboratory of Surface and Interface Chemistry and Energy Catalysis of Anhui Higher Education Institutes, University of Science and*

https://doi.org/10.1021/jacs.1c08284
J. Am. Chem. Soc. 2022, 144, 723−732

Technology of China, Hefei 230029, P. R. China; Donostia International Physics Center, San Sebastián 20018, Spain; Centro de Fisica de Materiales, CFM/MPC, CSIC-UPV/EHU, San Sebastián 20018, Spain; orcid.org/0000-0002-6545-5028; Email: taowang@dipc.org

Jean-Sabin McEwen − *The Gene & Linda Voiland School of Chemical Engineering and Bioengineering, Department of Physics and Astronomy, Department of Chemistry, and Department of Biological Systems Engineering, Washington State University, Pullman, Washington 99164, United States; Institute for Integrated Catalysis, Pacific Northwest National Laboratory, Richland, Washington 99352, United States;* orcid.org/0000-0003-0931-4869; Email: js.mcewen@wsu.edu

Junfa Zhu − *National Synchrotron Radiation Laboratory, Department of Chemical Physics and Key Laboratory of Surface and Interface Chemistry and Energy Catalysis of Anhui Higher Education Institutes, University of Science and Technology of China, Hefei 230029, P. R. China;* orcid.org/0000-0003-0888-4261; Email: jfzhu@ustc.edu.cn

Authors

Zhiwen Zeng − *National Synchrotron Radiation Laboratory, Department of Chemical Physics and Key Laboratory of Surface and Interface Chemistry and Energy Catalysis of Anhui Higher Education Institutes, University of Science and Technology of China, Hefei 230029, P. R. China*

Dezhou Guo − *The Gene & Linda Voiland School of Chemical Engineering and Bioengineering, Washington State University, Pullman, Washington 99164, United States*

Qifan Chen − *Institute of Physics of the Czech Academy of Sciences, 16200 Prague 6, Czechia*

Adam Matěj − *Institute of Physics of the Czech Academy of Sciences, 16200 Prague 6, Czechia*

Jianmin Huang − *National Synchrotron Radiation Laboratory, Department of Chemical Physics and Key Laboratory of Surface and Interface Chemistry and Energy Catalysis of Anhui Higher Education Institutes, University of Science and Technology of China, Hefei 230029, P. R. China*

Dong Han − *National Synchrotron Radiation Laboratory, Department of Chemical Physics and Key Laboratory of Surface and Interface Chemistry and Energy Catalysis of Anhui Higher Education Institutes, University of Science and Technology of China, Hefei 230029, P. R. China*

Qian Xu − *National Synchrotron Radiation Laboratory, Department of Chemical Physics and Key Laboratory of Surface and Interface Chemistry and Energy Catalysis of Anhui Higher Education Institutes, University of Science and Technology of China, Hefei 230029, P. R. China*

Aidi Zhao − *School of Physical Science and Technology, ShanghaiTech University, Shanghai 201210, P. R. China;* orcid.org/0000-0002-6546-4610

Pavel Jelínek − *Institute of Physics of the Czech Academy of Sciences, 16200 Prague 6, Czechia;* orcid.org/0000-0002-5645-8542

Dimas G. de Oteyza − *Donostia International Physics Center, San Sebastián 20018, Spain; Centro de Fisica de Materiales, CFM/MPC, CSIC-UPV/EHU, San Sebastián 20018, Spain; Ikerbasque, Basque Foundation for Science, 48013 Bilbao, Spain;* orcid.org/0000-0001-8060-6819

Complete contact information is available at: https://pubs.acs.org/10.1021/jacs.1c08284

Author Contributions

⬡Z.Z. and D.G. contributed equally.

Notes

The authors declare no competing financial interest.

■ ACKNOWLEDGMENTS

This work was financially supported by the National Natural Science Foundation of China (21773222, 51772285, 21872131, U1732272, and U1932214), the National Key R&D Program of China (2017YFA0403402, 2017YFA0403403, and 2019YFA0405601), and Users with Excellence Program of Hefei Science Center CAS (2020HSC-UE004). The work at Washington State University was primarily funded through the National Science Foundation CAREER program under Contract no. CBET-1653561. This work was also partially funded by the Joint Center for Deployment and Research in Earth Abundant Materials (JCDREAM) in Washington State. Most of the computational resources were provided by the Kamiak HPC under the Center for Institutional Research Computing at Washington State University. A portion of the computer time for the computational work was performed using EMSL, a national scientific user facility sponsored by the Department of Energy's Office of Biological and Environmental Research and located at Pacific Northwest National Laboratory. This research also used resources of the National Energy Research Scientific Computing Center (NERSC), a U.S. Department of Energy Office of Science User Facility operated under Contract no. DE-AC02-05CH11231. The work at Donostia International Physics Center was primarily funded through the Juan de la Cierva Grant (no. FJC2019-041202-I) from Spanish Ministry of Economy and Competitiveness, the European Union's Horizon 2020 Research and Innovation program (Marie Skłodowska-Curie Actions Individual Fellowship (no. 101022150), and the MCIN/AEI/ 10.13039/501100011033 (Grant no. PID2019-107338RB-C63).

■ REFERENCES

(1) Clair, S.; de Oteyza, D. G. Controlling a Chemical Coupling Reaction on a Surface: Tools and Strategies for On-Surface Synthesis. *Chem. Rev.* **2019**, *119*, 4717−4776.

(2) Wang, T.; Zhu, J. F. Confined On-Surface Organic Synthesis: Strategies and Mechanisms. *Surf. Sci. Rep.* **2019**, *74*, 97−140.

(3) Han, D.; Zhu, J. F. Surface-Assisted Fabrication of Low-Dimensional Carbon-Based Nanoarchitectures. *J. Phys.: Condens. Matter* **2021**, *33*, 343001.

(4) Li, Q.; Gao, J.; Li, Y.; Fuentes-Cabrera, M.; Liu, M.; Qiu, X.; Lin, H.; Chi, L.; Pan, M. Self-Assembly Directed One-Step Synthesis of [4] Radialene on Cu(100) Surfaces. *Nat. Commun.* **2018**, *9*, 3113.

(5) Chen, Q.; Cramer, J. R.; Liu, J.; Jin, X.; Liao, P.; Shao, X.; Gothelf, K. V.; Wu, K. Steering On-Surface Reactions by a Self-Assembly Approach. *Angew. Chem., Int. Ed.* **2017**, *56*, 5026−5030.

(6) Wang, T.; Huang, J.; Lv, H.; Fan, Q.; Feng, L.; Tao, Z.; Ju, H.; Wu, X.; Tait, S. L.; Zhu, J. Kinetic Strategies for the Formation of Graphyne Nanowires via Sonogashira Coupling on Ag(111). *J. Am. Chem. Soc.* **2018**, *140*, 13421−13428.

(7) Liu, W.; Luo, X.; Bao, Y.; Liu, Y. P.; Ning, G. H.; Abdelwahab, I.; Li, L.; Nai, C. T.; Hu, Z. G.; Zhao, D.; Liu, B.; Quek, S. Y.; Loh, K. P. A Two-Dimensional Conjugated Aromatic Polymer via C-C Coupling Reaction. *Nat. Chem.* **2017**, *9*, 563−570.

(8) Sánchez-Sánchez, C.; Dienel, T.; Deniz, O.; Ruffieux, P.; Berger, R.; Feng, X.; Müllen, K.; Fasel, R. Purely Armchair or Partially Chiral: Noncontact Atomic Force Microscopy Characterization of Dibromo-Bianthryl-Based Graphene Nanoribbons Grown on Cu(111). *ACS Nano* **2016**, *10*, 8006−8011.

(9) Kong, H.; Yang, S.; Gao, H.; Timmer, A.; Hill, J. P.; Diaz Arado, O. D.; Monig, H.; Huang, X.; Tang, Q.; Ji, Q.; Liu, W.; Fuchs, H. Substrate-Mediated C-C and C-H Coupling after Dehalogenation. *J. Am. Chem. Soc.* **2017**, *139*, 3669−3675.
(10) Shi, K. J.; Shu, C. H.; Wang, C. X.; Wu, X. Y.; Tian, H.; Liu, P. N. On-Surface Heck Reaction of Aryl Bromides with Alkene on Au(111) with Palladium as Catalyst. *Org. Lett.* **2017**, *19*, 2801−2804.
(11) Moreno, C.; Panighel, M.; Vilas-Varela, M.; Sauthier, G.; Tenorio, M.; Ceballos, G.; Peña, D.; Mugarza, A. Critical Role of Phenyl Substitution and Catalytic Substrate in the Surface-Assisted Polymerization of Dibromobianthracene Derivatives. *Chem. Mater.* **2019**, *31*, 331−341.
(12) Merino-Díez, N.; Pérez Paz, A.; Li, J.; Vilas-Varela, M.; Lawrence, J.; Mohammed, M. S. G.; Berdonces-Layunta, A.; Barragán, A.; Pascual, J. I.; Lobo-Checa, J.; Peña, D.; de Oteyza, D. G. Hierarchy in the Halogen Activation During Surface-Promoted Ullmann Coupling. *ChemPhysChem* **2019**, *20*, 2305−2310.
(13) Zhong, Q.; Ebeling, D.; Tschakert, J.; Gao, Y.; Bao, D.; Du, S.; Li, C.; Chi, L.; Schirmeisen, A. Symmetry Breakdown of 4,4″-Diamino-p-Terphenyl on a Cu(111) Surface by Lattice Mismatch. *Nat. Commun.* **2018**, *9*, 3277.
(14) Grill, L.; Dyer, M.; Lafferentz, L.; Persson, M.; Peters, M. V.; Hecht, S. Nano-Architectures by Covalent Assembly of Molecular Building Blocks. *Nat. Nanotechnol.* **2007**, *2*, 687−691.
(15) Cai, J.; Ruffieux, P.; Jaafar, R.; Bieri, M.; Braun, T.; Blankenburg, S.; Muoth, M.; Seitsonen, A. P.; Saleh, M.; Feng, X.; Müllen, K.; Fasel, R. Atomically Precise Bottom-Up Fabrication of Graphene Nanoribbons. *Nature* **2010**, *466*, 470−473.
(16) Zhou, X.; Wang, C.; Zhang, Y.; Cheng, F.; He, Y.; Shen, Q.; Shang, J.; Shao, X.; Ji, W.; Chen, W.; Xu, G.; Wu, K. Steering Surface Reaction Dynamics with a Self-Assembly Strategy: Ullmann Coupling on Metal Surfaces. *Angew. Chem., Int. Ed.* **2017**, *56*, 12852−12856.
(17) Feng, L.; Wang, T.; Jia, H.; Huang, J.; Han, D.; Zhang, W.; Ding, H.; Xu, Q.; Du, P.; Zhu, J. On-Surface Synthesis of Planar Acenes via Regioselective Aryl-Aryl Coupling. *Chem. Commun.* **2020**, *56*, 4890−4893.
(18) Rajca, A.; Safronov, A.; Rajca, S.; Ross, C. R.; Stezowski, J. J. Biphenylene Dimer. Molecular Fragment of a Two-Dimensional Carbon Net and Double-Stranded Polymer. *J. Am. Chem. Soc.* **1996**, *118*, 7272−7279.
(19) Zhang, C.; Kazuma, E.; Kim, Y. Atomic-Scale Visualization of the Stepwise Metal-Mediated Dehalogenative Cycloaddition Reaction Pathways: Competition between Radicals and Organometallic Intermediates. *Angew. Chem., Int. Ed.* **2019**, *58*, 17736−17744.
(20) Tran, B. V.; Pham, T. A.; Grunst, M.; Kivala, M.; Stohr, M. Surface-confined [2 + 2] cycloaddition towards one-dimensional polymers featuring cyclobutadiene units. *Nanoscale* **2017**, *9*, 18305−18310.
(21) Li, D. Y.; Qiu, X.; Li, S. W.; Ren, Y. T.; Zhu, Y. C.; Shu, C. H.; Hou, X. Y.; Liu, M.; Shi, X. Q.; Qiu, X.; Liu, P. N. Ladder Phenylenes Synthesized on Au(111) Surface via Selective [2 + 2] Cycloaddition. *J. Am. Chem. Soc.* **2021**, *143*, 12955−12960.
(22) Liu, M.; Liu, M.; She, L.; Zha, Z.; Pan, J.; Li, S.; Li, T.; He, Y.; Cai, Z.; Wang, J.; Zheng, Y.; Qiu, X.; Zhong, D. Graphene-like Nanoribbons Periodically Embedded with Four- and Eight-Membered Rings. *Nat. Commun.* **2017**, *8*, 14924.
(23) Zhang, R.; Xia, B.; Xu, H.; Lin, N. Identifying Multinuclear Organometallic Intermediates in On-Surface [2 + 2] Cycloaddition Reactions. *Angew. Chem., Int. Ed.* **2019**, *58*, 16485−16489.
(24) Fan, Q.; Yan, L.; Tripp, M. W.; Krejci, O.; Dimosthenous, S.; Kachel, S. R.; Chen, M.; Foster, A. S.; Koert, U.; Liljeroth, P.; Gottfried, J. M. Biphenylene network: A nonbenzenoid carbon allotrope. *Science* **2021**, *372*, 852−856.
(25) Sanchez-Sanchez, C.; Nicolai, A.; Rossel, F.; Cai, J.; Liu, J.; Feng, X.; Mullen, K.; Ruffieux, P.; Fasel, R.; Meunier, V. On-Surface Cyclization of ortho-Dihalotetracenes to Four- and Six-Membered Rings. *J. Am. Chem. Soc.* **2017**, *139*, 17617−17623.
(26) Sanchez-Sanchez, C.; Dienel, T.; Nicolai, A.; Kharche, N.; Liang, L.; Daniels, C.; Meunier, V.; Liu, J.; Feng, X.; Mullen, K.; Sanchez-Valencia, J. R.; Groning, O.; Ruffieux, P.; Fasel, R. On-Surface Synthesis and Characterization of Acene-Based Nanoribbons Incorporating Four-Membered Rings. *Chem. - Eur. J.* **2019**, *25*, 12074−12082.
(27) de Oteyza, D. G.; Garcia-Lekue, A.; Vilas-Varela, M.; Merino-Diez, N.; Carbonell-Sanroma, E.; Corso, M.; Vasseur, G.; Rogero, C.; Guitian, E.; Pascual, J. I.; Ortega, J. E.; Wakayama, Y.; Peña, D. Substrate-Independent Growth of Atomically Precise Chiral Graphene Nanoribbons. *ACS Nano* **2016**, *10*, 9000−9008.
(28) Wang, T.; Lv, H.; Huang, J.; Shan, H.; Feng, L.; Mao, Y.; Wang, J.; Zhang, W.; Han, D.; Xu, Q.; Du, P.; Zhao, A.; Wu, X.; Tait, S. L.; Zhu, J. Reaction Selectivity of Homochiral versus Heterochiral Intermolecular Reactions of Prochiral Terminal Alkynes on Surfaces. *Nat. Commun.* **2019**, *10*, 4122.
(29) Fan, Q.; Liu, L.; Dai, J.; Wang, T.; Ju, H.; Zhao, J.; Kuttner, J.; Hilt, G.; Gottfried, J. M.; Zhu, J. Surface Adatom Mediated Structural Transformation in Bromoarene Monolayers: Precursor Phases in Surface Ullmann Reaction. *ACS Nano* **2018**, *12*, 2267−2274.
(30) Simonov, K. A.; Generalov, A. V.; Vinogradov, A. S.; Svirskiy, G. I.; Cafolla, A. A.; McGuinness, C.; Taketsugu, T.; Lyalin, A.; Martensson, N.; Preobrajenski, A. B. Synthesis of Armchair Graphene Nanoribbons from The 10,10′-dibromo-9,9′-bianthracene Molecules on Ag(111): The Role of Organometallic Intermediates. *Surf. Sci. Rep.* **2018**, *8*, 3506.
(31) Abyazisani, M.; MacLeod, J. M.; Lipton-Duffin, J. Cleaning up after the Party: Removing the Byproducts of On-Surface Ullmann Coupling. *ACS Nano* **2019**, *13*, 9270−9278.
(32) Fan, Q. T.; Wang, C. C.; Liu, L. M.; Han, Y.; Zhao, J.; Zhu, J. F.; Kuttner, J.; Hilt, G.; Gottfried, J. M. Covalent, Organometallic, and Halogen-Bonded Nanomeshes from Tetrabromo-Terphenyl by Surface-Assisted Synthesis on Cu(111). *J. Phys. Chem. C* **2014**, *118*, 13018−13025.
(33) Wang, T.; Lv, H. F.; Feng, L.; Tao, Z. J.; Huang, J. M.; Fan, Q. T.; Wu, X. J.; Zhu, J. F. Unravelling the Mechanism of Glaser Coupling Reaction on Ag(111) and Cu(111) Surfaces: a Case for Halogen Substituted Terminal Alkyne. *J. Phys. Chem. C* **2018**, *122*, 14537−14545.
(34) Han, D.; Fan, Q. T.; Dai, J. Y.; Wang, T.; Huang, J. M.; Xu, Q.; Ding, H. H.; Hu, J.; Feng, L.; Zhang, W. Z.; Zeng, Z. W.; Gottfried, J. M.; Zhu, J. F. On-Surface Synthesis of Armchair-Edged Graphene Nanoribbons with Zigzag Topology. *J. Phys. Chem. C* **2020**, *124*, 5248−5256.
(35) Kawai, S.; Takahashi, K.; Ito, S.; Pawlak, R.; Meier, T.; Spijker, P.; Canova, F. F.; Tracey, J.; Nozaki, K.; Foster, A. S.; Meyer, E. Competing Annulene and Radialene Structures in a Single Anti-Aromatic Molecule Studied by High-Resolution Atomic Force Microscopy. *ACS Nano* **2017**, *11*, 8122−8130.
(36) Hieulle, J.; Carbonell-Sanromà, E.; Vilas-Varela, M.; Garcia-Lekue, A.; Guitián, E.; Peña, D.; Pascual, J. I. On-Surface Route for Producing Planar Nanographenes with Azulene Moieties. *Nano Lett.* **2018**, *18*, 418−423.
(37) Wang, T.; Fan, Q.; Feng, L.; Tao, Z.; Huang, J.; Ju, H.; Xu, Q.; Hu, S.; Zhu, J. Chiral Kagome Lattices from On-Surface Synthesized Molecules. *ChemPhysChem* **2017**, *18*, 3329−3333.
(38) Wang, T.; Lawrence, J.; Sumi, N.; Robles, R.; Castro-Esteban, J.; Rey, D.; Mohammed, M. S. G.; Berdonces-Layunta, A.; Lorente, N.; Pérez, D.; Peña, D.; Corso, M.; de Oteyza, D. G. Challenges in the Synthesis of Corannulene-Based Non-Planar Nanographenes on Au(111) Surfaces. *Phys. Chem. Chem. Phys.* **2021**, *23*, 10845−10851.
(39) Beniwal, S.; Chen, S.; Kunkel, D. A.; Hooper, J.; Simpson, S.; Zurek, E.; Zeng, X. C.; Enders, A. Kagome-like Lattice of pi-pi Stacked 3-Hydroxyphenalenone on Cu(111). *Chem. Commun.* **2014**, *50*, 8659−62.
(40) Inayeh, A.; Groome, R. R. K.; Singh, I.; Veinot, A. J.; de Lima, F. C.; Miwa, R. H.; Crudden, C. M.; McLean, A. B. Self-Assembly of N-Heterocyclic Carbenes on Au(111). *Nat. Commun.* **2021**, *12*, 4034.
(41) Fan, Q.; Gottfried, J. M.; Zhu, J. Surface-Catalyzed C-C Covalent Coupling Strategies toward the Synthesis of Low-Dimen-

https://doi.org/10.1021/jacs.1c08284
J. Am. Chem. Soc. 2022, 144, 723−732

sional Carbon-Based Nanostructures. *Acc. Chem. Res.* **2015**, *48*, 2484−2494.
(42) Jelínek, P. High Resolution SPM Imaging of Organic Molecules With Functionalized Tips. *J. Phys.: Condens. Matter* **2017**, *29*, 343002−343019.
(43) Randić, M.; Balaban, A. T.; Plavšić, D. Applying the Conjugated Circuits Method to Clar Structures of [n] Phenylenes for Determining Resonance Energies. *Phys. Chem. Chem. Phys.* **2011**, *13*, 20644−20648.
(44) Rosenberg, M.; Dahlstrand, C.; Kilsa, K.; Ottosson, H. Excited State Aromaticity and Antiaromaticity: Opportunities for Photophysical and Photochemical Rationalizations. *Chem. Rev.* **2014**, *114*, 5379−5425.
(45) Barron, T. H. K.; Barton, J. W.; Johnson, J. D. On the stability of some polycyclic biphenylene derivatives. *Tetrahedron* **1966**, *22*, 2609−2613.
(46) Yokozeki, A.; Wilcox, C. F.; Bauer, S. H. Biphenylene. Internuclear Distances and Their Root Mean Square Amplitudes of Vibration. *J. Am. Chem. Soc.* **1974**, *96*, 1026−1032.
(47) Schmidt-Radde, R. H.; Vollhardt, K. P. C. The Total Synthesis of Angular [4]- and [5] Phenylene. *J. Am. Chem. Soc.* **1992**, *114*, 9713−9715.
(48) Baldridge, K. K.; Siegel, J. S. Bond Alternation in Triannelated Benzenes: Dissection of Cyclic. Pi. from Mills-Nixon Effects. *J. Am. Chem. Soc.* **1992**, *114*, 9583−9587.
(49) Faust, R.; Glendening, E. D.; Streitwieser, A.; Vollhardt, K. P. C. Ab Initio Study of. Sigma.- and. Pi.-Effects in Benzenes Fused to Four-Membered Rings: Rehybridization, Delocalization, and Antiaromaticity. *J. Am. Chem. Soc.* **1992**, *114*, 8263−8268.
(50) Bürgi, H.-B.; Baldridge, K. K.; Hardcastle, K.; Frank, N. L.; Gantzel, P.; Siegel, J. S.; Ziller, J. X-Ray Diffraction Evidence for a Cyclohexatriene Motif in the Molecular Structure of Tris-(bicyclo[2.1.1]hexeno)benzene: Bond Alternation after the Refutation of the Mills−Nixon Theory. *Angew. Chem., Int. Ed. Engl.* **1995**, *34*, 1454−1456.
(51) Vollhardt, K. P. C. The Phenylenes. *Pure Appl. Chem.* **1993**, *65*, 153−156.
(52) Gross, L.; Mohn, F.; Moll, N.; Schuler, B.; Criado, A.; Guitian, E.; Pena, D.; Gourdon, A.; Meyer, G. Bond-Order Discrimination by Atomic Force Microscopy. *Science* **2012**, *337*, 1326−9.
(53) Pozo, I.; Majzik, Z.; Pavlicek, N.; Melle-Franco, M.; Guitian, E.; Pena, D.; Gross, L.; Perez, D. Revisiting Kekulene: Synthesis and Single-Molecule Imaging. *J. Am. Chem. Soc.* **2019**, *141*, 15488−15493.
(54) Setiawan, D.; Kraka, E.; Cremer, D. Quantitative Assessment of Aromaticity and Antiaromaticity Utilizing Vibrational Spectroscopy. *J. Org. Chem.* **2016**, *81*, 9669−9686.
(55) Schleyer, P. V. R.; Maerker, C.; Dransfeld, A.; Jiao, H.; van Eikema Hommes, N. J. R. Nucleus-Independent Chemical Shifts: A Simple and Efficient Aromaticity Probe. *J. Am. Chem. Soc.* **1996**, *118*, 6317−6318.
(56) Herges, R.; Geuenich, D. Delocalization of Electrons in Molecules. *J. Phys. Chem. A* **2001**, *105*, 3214−3220.
(57) Björk, J. Reaction Mechanisms for On-Surface Synthesis of Covalent Nanostructures. *J. Phys.: Condens. Matter* **2016**, *28*, 083002.
(58) Di Giovannantonio, M.; Tomellini, M.; Lipton-Duffin, J.; Galeotti, G.; Ebrahimi, M.; Cossaro, A.; Verdini, A.; Kharche, N.; Meunier, V.; Vasseur, G.; Fagot-Revurat, Y.; Perepichka, D. F.; Rosei, F.; Contini, G. Mechanistic Picture and Kinetic Analysis of Surface-Confined Ullmann Polymerization. *J. Am. Chem. Soc.* **2016**, *138*, 16696−16702.
(59) Björk, J.; Hanke, F.; Stafstrom, S. Mechanisms of Halogen-Based Covalent Self-Assembly on Metal Surfaces. *J. Am. Chem. Soc.* **2013**, *135*, 5768−5575.
(60) Huang, J.; Pan, Y.; Wang, T.; Cui, S.; Feng, L.; Han, D.; Zhang, W.; Zeng, Z.; Li, X.; Du, P.; Wu, X.; Zhu, J. Topology Selectivity in On-Surface Dehydrogenative Coupling Reaction: Dendritic Structure versus Porous Graphene Nanoribbon. *ACS Nano* **2021**, *15*, 4617−4626.
(61) Cirera, B.; Giménez-Agulló, N.; Björk, J.; Martínez-Peña, F.; Martin-Jimenez, A.; Rodriguez-Fernandez, J.; Pizarro, A. M.; Otero, R.; Gallego, J. M.; Ballester, P.; Galan-Mascaros, J. R.; Ecija, D. Thermal Selectivity of Intermolecular versus Intramolecular Reactions on Surfaces. *Nat. Commun.* **2016**, *7*, 11002.
(62) Lin, T.; Zhang, L.; Björk, J.; Chen, Z.; Ruben, M.; Barth, J. V.; Klappenberger, F. Terminal Alkyne Coupling on a Corrugated Noble Metal Surface: From Controlled Precursor Alignment to Selective Reactions. *Chem. - Eur. J.* **2017**, *23*, 15588−15593.

NOTE ADDED AFTER ASAP PUBLICATION

After this paper was published ASAP December 29, 2021, a correction was made to Figure 2l. The corrected version was reposted January 4, 2022.

Recommended by ACS

Steering Surface Reaction at Specific Sites with Self-Assembly Strategy
Xiong Zhou, Kai Wu, *et al.*
AUGUST 15, 2017
ACS NANO
READ

On-Surface Synthesis of a Five-Membered Carbon Ring from a Terminal Alkynyl Bromide: A [4 + 1] Annulation
Tao Wang, Junfa Zhu, *et al.*
JULY 07, 2020
THE JOURNAL OF PHYSICAL CHEMISTRY LETTERS
READ

Unravelling the Mechanism of Glaser Coupling Reaction on Ag(111) and Cu(111) Surfaces: a Case for Halogen Substituted Terminal Alkyne
Tao Wang, Junfa Zhu, *et al.*
JUNE 11, 2018
THE JOURNAL OF PHYSICAL CHEMISTRY C
READ

Controllable Density of Atomic Bromine in a Two-Dimensional Hydrogen Bond Network
Jianchen Lu, Hong-Jun Gao, *et al.*
OCTOBER 17, 2018
THE JOURNAL OF PHYSICAL CHEMISTRY C
READ

Get More Suggestions >

https://doi.org/10.1021/jacs.1c08284
J. Am. Chem. Soc. 2022, 144, 723−732